metals

Article

Effect of α Phase on Dynamic Mechanical Properties and Failure of Ti-4Al-5Mo-5V-5Cr-1Nb Alloy after Two-Stage Aging

Tao Wang [1,2,*], Xianghong Liu [2], Yong Feng [1,2], Kaixuan Wang [2], Shangqing Sun [2], Dong Yang [2] and Feng Sun [2]

[1] State Key Laboratory of Solidification Processing, Northwestern Polytechnical University, Xi'an 710072, China
[2] Western Superconducting Technologies Co., Ltd., Xi'an 710018, China
* Correspondence: wang_tao@c-wst.com

Abstract: This work studied the high strain rate behavior of the Ti-4Al-5Mo-5V-5Cr-1Nb (Ti-45551) alloy after two-stage aging, with dynamic tension tests conducted using the split Hopkinson tensile bar. The results show that the microstructure, especially the size and distribution of the α phase, significantly affects the mechanical and failure behaviors of the Ti-45551 alloy under dynamic loading. As the strain rate increases, increasing trends can be observed in both ductility and strength, which is intimately related to the activation of the dislocation slip in the α phase. Moreover, obvious strain softening was found in the Ti-45551 alloy under dynamic loading. In this study, the microstructure observations suggest that dislocation slips are highly active in the α phase under dynamic loading. Fractographic characterization of the fracture surfaces under dynamic loading reveals a uniform distribution of ductile dimples, which indicates that a uniform distribution of the nano-scale α phase can effectively reduce brittle fracture tendency. Our studies provide a comprehensive picture of how strain rate drives dynamic plasticity and failure mode in the Ti alloy.

Keywords: metastable β-Ti alloys; strain rate effect; phase distribution; mechanical properties

check for updates

Citation: Wang, T.; Liu, X.; Feng, Y.; Wang, K.; Sun, S.; Yang, D.; Sun, F. Effect of α Phase on Dynamic Mechanical Properties and Failure of Ti-4Al-5Mo-5V-5Cr-1Nb Alloy after Two-Stage Aging. *Metals* **2022**, *12*, 1721. https://doi.org/10.3390/met12101721

Academic Editor: Carlos Capdevila-Montes

Received: 16 August 2022
Accepted: 10 October 2022
Published: 14 October 2022

1. Introduction

As Titanium alloys have many excellent properties, such as high strength-to-weight ratio, high toughness, good biocompatibility and outstanding damage tolerance, they have been widely used in the aviation, marine and automotive industries [1–3]. In recent years, metastable β-Ti alloys have become more and more promising, due to their excellent combination of strength and ductility [4]. Additionally, metastable β-Ti alloys have been widely used in biomedicine, due to their elastic modulus being comparable to human bone, and in heavy aerospace components [5,6], which usually need to take into account dynamic mechanical behaviors and failure modes [7]. Therefore, it is very important to study the dynamic mechanical behaviors and failure mode of metastable β-Ti alloys under dynamic loading conditions.

It is widely known that mechanical behaviors of Ti alloys rely on the presence and distribution of the α phase, which is very sensitive to deformation temperature, strain rate and strain value in the forging process [8–10]. Through different thermomechanical processes, various microstructures can be produced [11–13]. To date, many studies have been performed to investigate microstructures on mechanical behaviors of metastable β-Ti alloys [14,15]. Generally, metastable β-Ti alloys with an equiaxed α phase exhibit good ductility under quasi-static loading [16]. This is because the equiaxed α phase shows good compatibility during plastic deformation. However. under shock loading, dislocation sliding in the β phase (body-centered cubic, bcc) still contributes much more plastic deformation than the α phase (twinning) [17]. Chen et al. studied the influence of the α phase on the dynamic failure mode and pointed out that an elongated α phase close to the localized shear region finally formed parabolic dimples with further plastic deformation [18]. The volume fraction, size and distribution of the α phase exhibit great effects on the dynamic behaviors of metastable β-Ti alloys [19]. Nonetheless, little experimental data exists in the literature about the effect of the lamellar α phase, a regular α + β microstructure, on dynamic plasticity and failure of metastable β-Ti alloys. Thus, the effect of the phase composition on dynamic plastic deformation and mechanical behaviors of metastable β-Ti alloys should be studied.

The objective of this study is to investigate the dynamic mechanical behaviors, deformation mechanisms and failure modes of metastable β-Ti alloys with a lamellar α phase under dynamic loading at a range of high strain rates (>600 s^{-1}). Therefore, different heat treatments, such as two-stage aging, were applied to the metastable β-Ti alloys in order to obtain a uniform distribution of the lamellar α phase. Subsequently, dynamic tensile tests were conducted at room temperature. In this work, a series of quasi-static and Split Hopkinson tension bar experiments were conducted on a Ti-45551 alloy, to investigate the dynamic mechanical behaviors. Both mechanical behaviors (dynamic plasticity and failure mode) and the underlying deformation mechanisms are discussed. The influence of microstructure and phase composition on the plastic deformation mechanisms operating under quasi-static and dynamic tensile loading are systematically investigated.

2. Experimental

2.1. Sample Preparation

The received Ti-45551 ingot smelted by vacuum self-consumable arc melting (VAR) was forged in β-field and then α + β field by a hydraulic press, and Table 1 shows its chemical composition. The β-transus temperature of the ingot Ti-45551 was approximately 800 °C. After multi-axial α + β field forging, the microstructure of Ti-45551 was as shown in Figure 1a,b. The β-field forging and the multi-axial α +β field forging were conducted at 785 °C [3]. Ti-45551 alloy exhibits a typical equiaxed primary α (α_p) + secondary α (α_s) lamellae + β bimodal microstructure. In addition, there were a lot of dislocations around the lamellar α_s phase, due to the forging process. To obtain a typical lamellar α_s phase, a solution heat treatment at 870 °C for 2 h was performed, and followed by air cooling (AC), and then aged at 360 °C for 8 h and AC and followed by another aging at 550 °C for 8 h. Figure 2 shows that the applied heated treatment resulted in the formation of uniform distribution of the α_s lamellar microstructure or martensite microstructure. The number density of the lamellar α_s phase is very high, and there is no obvious equiaxed α phase. In addition, the energy dispersive X-ray spectroscopy (EDX) maps (Figure 2d–g) show that the elements have a uniform distribution in Ti-45551, a result obtained by using a JEOL 4700 scanning electron microscope (SEM).

Table 1. Chemical composition of T-45551 titanium alloy (wt.%).

Position	Chemical Composition (wt.%)									
	Al	Mo	V	Cr	Nb	C	N	O	H	Ti
Top	4.00	4.99	5.03	5.01	1.03	0.005	0.007	0.107	0.0006	bal.
Middle	3.98	5.02	5.01	5.04	1.05	0.005	0.004	0.105	0.0004	bal.
Bottom	4.03	4.97	5.04	5.02	1.01	0.005	0.006	0.107	0.0007	bal.

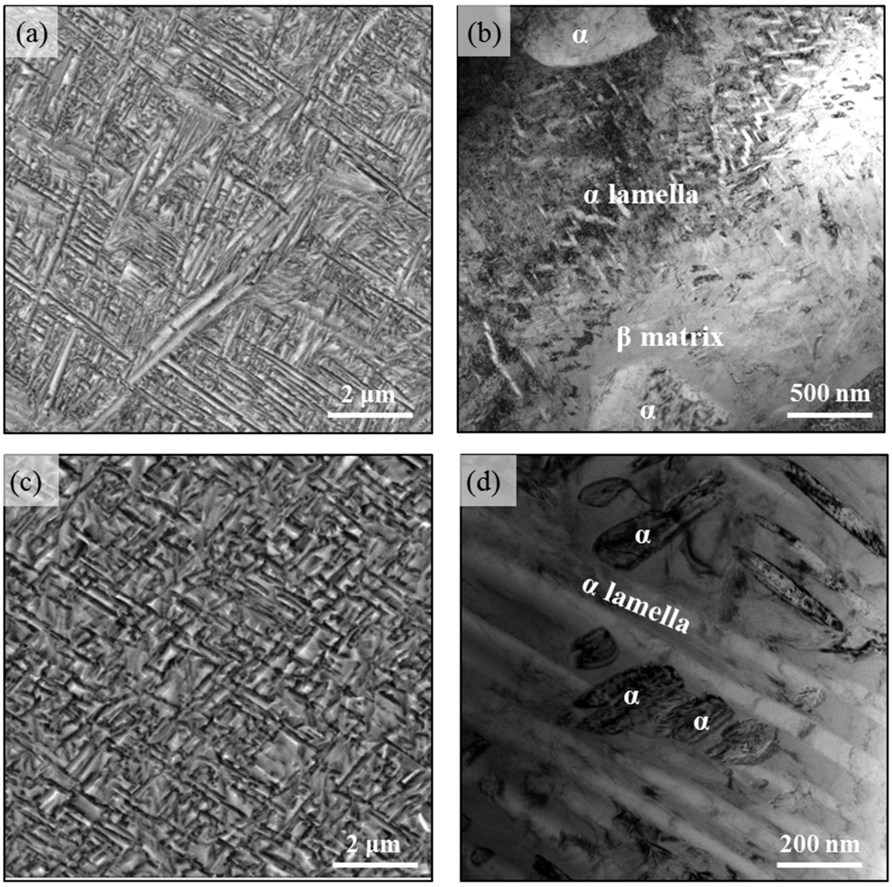

Figure 1. Typical microstructure of the metastable β-Ti alloys after forging in β-field and multi-axial α + β field. (**a**) SEM micrograph, (**b**) bright field TEM micrograph and microstructures after one stage aging, (**c**) SEM micrograph, (**d**) bright field TEM micrograph.

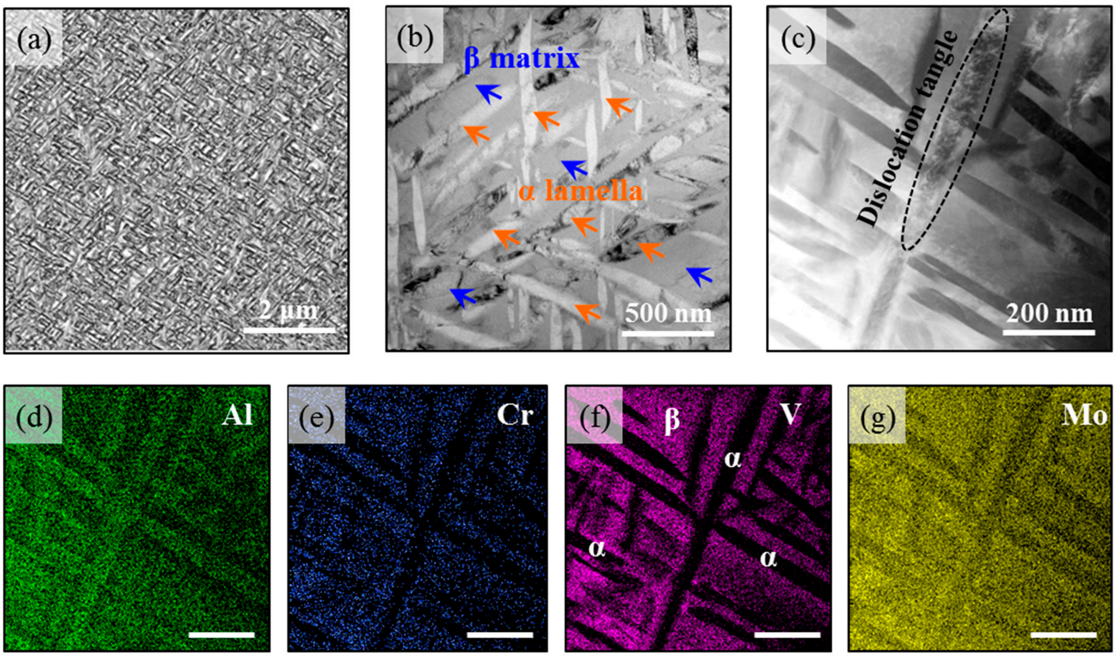

Figure 2. The microstructure of Ti-45551 alloy after two-stage aging, (**a**) optical micrograph, (**b**) TEM and (**c**) HAADF images of phase shape and distribution, (**d**–**g**) XEDS concentration maps showing the chemical composition distribution of Al, Cr, V, and Mo in in the β and α phases, respectively.

2.2. Characterization Methods

In this work, before and after tensile tests the samples were cut into a piece along the cross-section and then prepared for microstructure characterizations. To investigate microstructure evolution under different processing conditions, slices for TEM were cut form the specimens. For TEM characterization, the Ti-45551 alloy samples used mechanical polishing to reach approximately 50 µm thickness, and were prepared using a twin-jet electro-polisher in an acetic acid solution containing 10 vol.% perchloric acid at 25 mA and 20 °C. A FEI Talos F200X transmission electron microscope (TEM) operating at 200 kV was used for bright-field images and a high-angle annular dark field (HADDF) investigated the microstructure before and after plastic deformation.

After quasi-static and dynamic tensile tests, a JSM-IT700R field emission SEM was used to characterize the surface fracture morphology.

2.3. Mechanical Properties

Mechanical properties were conducted using an electronic universal testing machine and Split Hopkinson Tension Bar (SHTB) at room temperature. The specimens were tested with strain rate at $1 \times 10^{-3}\ s^{-1}$, $6 \times 10^{2}\ s^{-1}$, $2 \times 10^{3}\ s^{-1}$ and $4 \times 10^{3}\ s^{-1}$. Dynamic tensile tests were performed with a classic Split Hopkinson Tension Bar (SHTB), as shown in Figure 3. The SHTB system consists of an absorption bar, steel tube striker, incident bar, transmission bars, and strain gages.

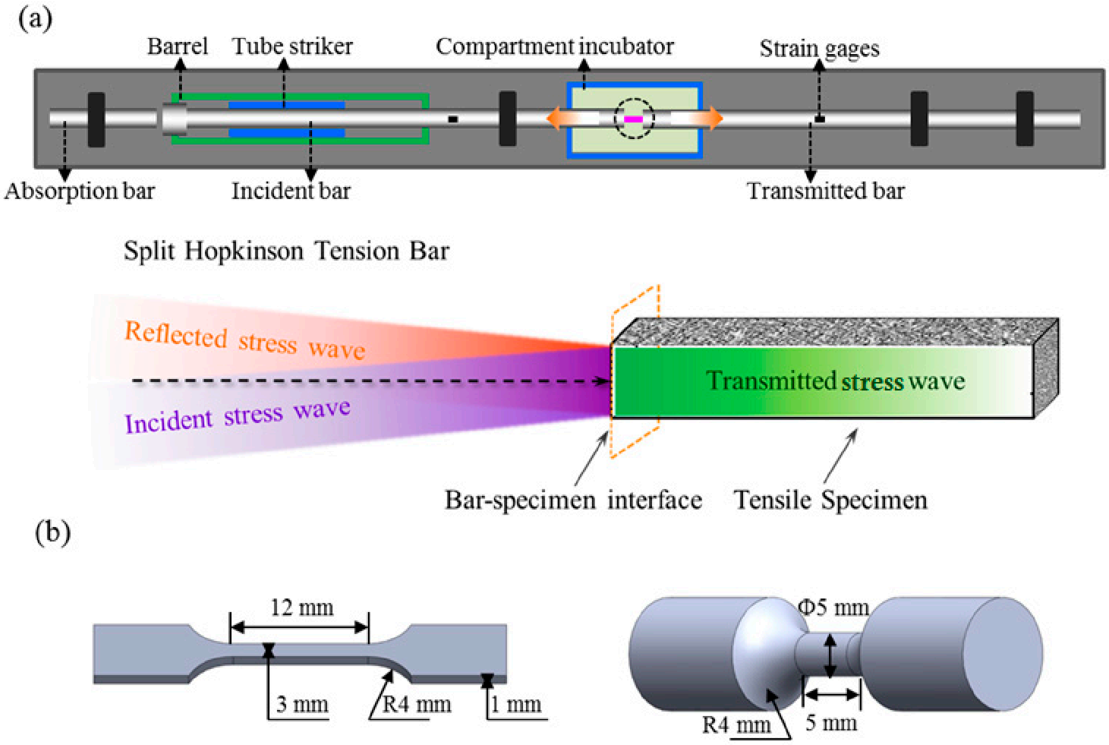

Figure 3. (**a**) Schematic illustration of Split Hopkinson Tension Bar (SHPB) system and a typical set of stress waves during dynamic tension. (**b**) The precise dimensions of the Ti-45551 alloy samples for quasi-static and dynamic tensile tests.

During the test, at the time that the strike bar in the chamber of the tube impacted the incident bar at a certain speed, an incident pulse was generated in the incident bar (ϕ 12.7 mm, 1.5 m). The stress wave reached the specimen through the elastic incident bar, and the specimen was deformed at high speed, under the action of the stress pulse. The stress wave simultaneously generated a reflected pulse through the specimen, entered the elastic incident bar, and the projected pulse entered the transmitted bar (ϕ 12.7 mm, 1.5 m). The tachometer is able to obtain the strike velocity of a bullet, paste the strain gauge on the elastic bar, and record the strain pulse to calculate the dynamic stress and strain parameters of the material. Based on the one–dimensional stress wave theory, the true stress, true strain and strain rate of each impact can be calculated as follows:

$$\sigma_S(t) = E\left(\frac{A}{A_S}\right)\varepsilon_T(t) \tag{1}$$

$$\varepsilon_S(t) = \frac{2C_0}{l_S}\int_0^t \varepsilon_R(t)dt \tag{2}$$

$$\acute{\varepsilon}_S(t) = \frac{2C_0}{l_S}\varepsilon_R(t) \tag{3}$$

The ε_R and the ε_T are reflection and transmission strain pulses. E is Young's modulus; A is the cross-sectional area; C_0 is the longitudinal wave speed of the bars; A_s is the cross-sectional area of the specimen and l_s is the length of the specimen. The details of the SHTB technique can be found elsewhere [20,21]. The precise dimensions of Ti-45551 samples for quasi-static (12 mm × 3 mm × 1 mm) and dynamic (ϕ5 mm × 5 mm) are illustrated in Figure 3b. For every single valid stress-strain curve, three tests were performed under the same loading conditions.

3. Results and Discussion

3.1. Microstructure Evolution after Two Stage Aging

Figure 1a shows the microscopy of Ti-45551 after multi-axial α + β field forging. Based on the SEM image, the α phase precipitates exhibit a darker contrast, due to their higher Al content and lower Mo content. It can be seen that the α phase precipitates shows two clearly different morphologies, namely the equiaxed α_p phase and the lamellar α_s phase, as shown in Figure 1b. After one stage aged at 360 °C for 8 h, the α phase precipitates became finer, and the density of the equiaxed α_p phase decreases as shown in Figure 1b,c. After two stages of aging, the Ti-45551 sample showed a uniform fine lamellar α_s phase microstructure and there was no equiaxed α_p phase, as shown in Figure 2. The length of the lamellar α_s phase was approximately 200 nm to 2 µm, while its width was approximately 30–60 nm, as seen in Figure 3b,c. The element distribution is shown in Figure 3d–g.

3.2. Mechanical Performance

During dynamic loading, one surface of the specimen was driven inwards with an incident stress wave (marked in a purple color, with a wave speed f roughly 4.966 m/s), and then deformed and failure with transmitted stress wave (marked in a green color), as illustrated in Figure 3. The true stress-strain curves at different strain rates presented different patterns, as shown in Figure 3a. Under quasi-static loading conditions, the lamellar α_s + β phase Ti-45551 shows clearly a strain hardening capability, as shown in Figure 4a. The yield strength (σ_y) is around 1100 MPa and the failure strain (ε_f) is approximately 6.1%. Under dynamic loading, the samples exhibit higher yield strength, due to the strain-rate effect and larger ductility. In addition, under quasi-static loading the Ti-45551 shows an obvious strain hardening capability, with the stress increasing with straining. But under dynamic loading, after yielding, the stress gradually decreases with straining. This transition from strain hardening to strain softening is mainly due to the changing of the deformation modes. The Ti-45551 alloy exhibits obvious positive strain rate sensitivity, as shown in Figure 4b. The yield stress increases with increasing strain rate.

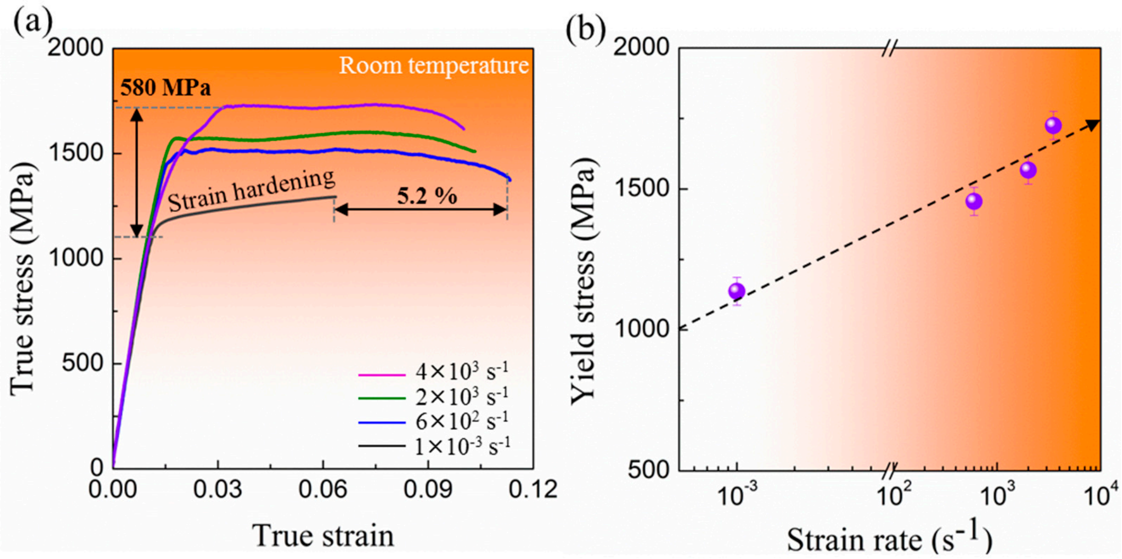

Figure 4. (**a**) The true stress-strain curves at 1×10^{-3}, 6×10^{2}, 2×10^{3} and 4×10^{3} s^{-1} presented different patterns of Ti-45551 alloy after two-stage aging at room temperature. (**b**) The relationship between yield strength at room temperature and strain rate.

3.3. Deformation Mechanisms

For Ti alloys, the plasticity of lamellar microstructure is primarily controlled by slip and shearing [22]. At room temperature, the lamellar α phase has only two independent slip systems, due to its hexagonal close-packed (hcp) crystalline structure [23]. Therefore, the ductility of the lamellar α + β phase Ti-45551 largely depends on the deformation capability of the lamellar α phase.

Before quasi-static loading, the microstructure of Ti-5551 is shown in Figures 2b and 5a. In the lamellar α_s phase, the dislocation density is very low, due to the heat treatment. Under quasi-static loading, a few dislocations can be found in the α_s lamellae and a relatively higher dislocation density structure primarily locates in the β phase, as shown in Figure 5b. This is due to the limited slip systems in the hcp α_s phase, which exhibit higher critical shear stress. Meanwhile, high density dislocations are stacked in the β phase around an α lamellae structure, which blocks the motion of dislocations. Furthermore, some α/β interfaces are still clear, which means that no dislocations are activated to form α/β interfaces. Therefore, this uninform dislocation slip mode in α and β phases introduces low ductility in Ti-45551 at quasi-static loading.

Under dynamic loading, the deformation mechanisms are totally changed. As shown in Figure 6a, many dislocations are activated from α/β interfaces and in the α lamellae. This is because under high-strain-rate loading, the slip systems nucleate in the α and β phases, due to high stress waves. Therefore, the α lamellas can also contribute more plastic deformation. Under shock loading, dislocation nucleation is a typical deformation mode, which always occurs at a high stress state [24]. As the stress increases, many dislocations are activated in both the α and β phases, which will lead to the uniform distribution of high density dislocation structures in a deformed region, see Figure 6b. The α lamellas are full of slip lines and dislocation tangles (Figure 6c). Therefore, the lamellar α + β phase Ti-45551 can exhibit large ductility under dynamic loading conditions. In addition, we also found some deformation twinning in the α lamellas, due to the high strain rate. This deformation twinning can also contribute to the whole plastic deformation, as shown in Figure 6d.

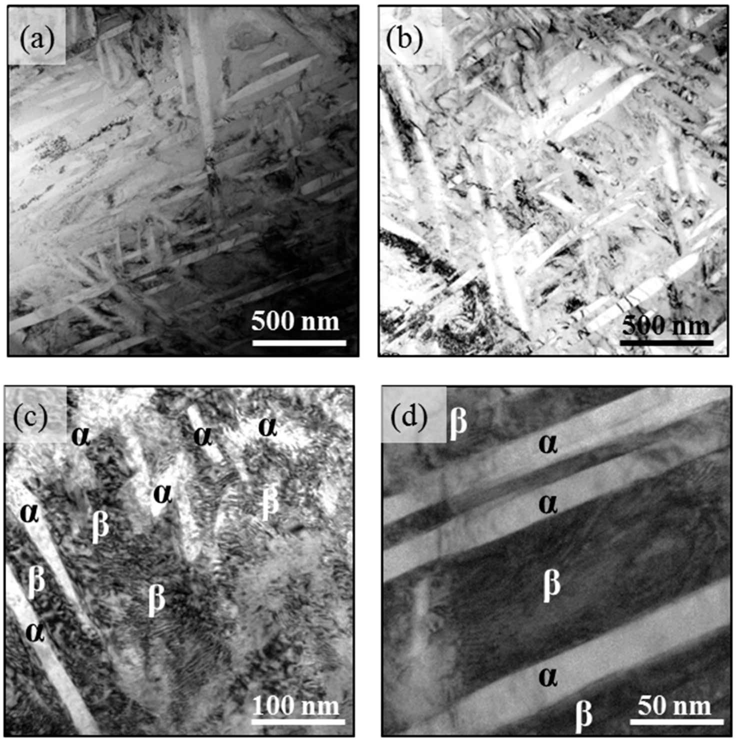

Figure 5. Microstructure of Ti-45551 alloy before quasi-static loading (**a**) and deformation micromechanisms after quasi-static loading. TEM image of the cross-section of the deformation zones at (**a**) quasi-static, and its details (**b**–**d**).

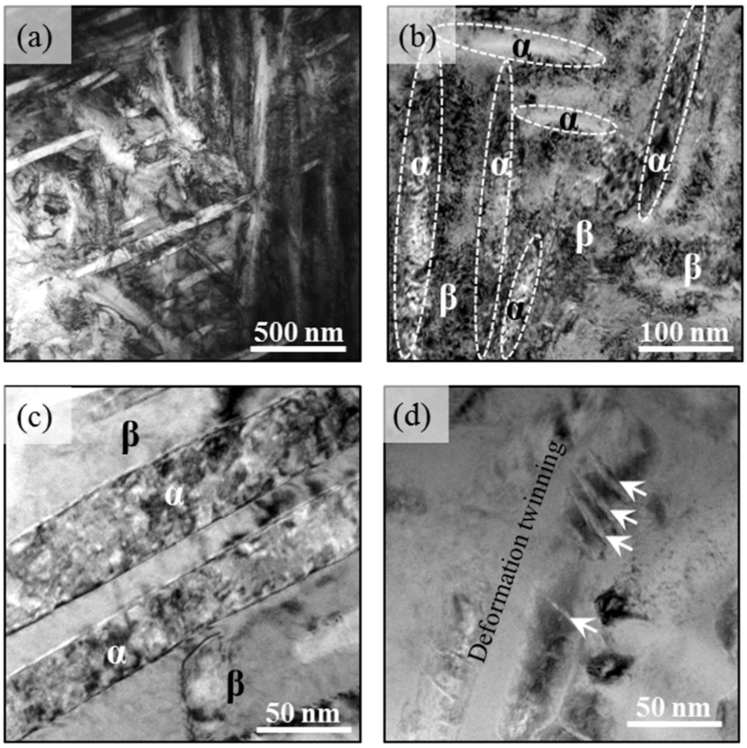

Figure 6. Deformation micromechanisms in the Ti-45551 alloy at dynamic loading. TEM image of the cross-section of the deformation zones at (**a**) quasi-static, and its details (**b**–**d**).

3.4. Failure Modes

Figure 7a shows the fractography of the quasi-static tension specimen. A failure mode mix of dimples and cracks can be seen. There are a lot of dimples and clear cracks in the center area of the fracture surface. Under dynamic loading, there are more fine dimples and less crack edge, which corresponds to good ductility, and which can be seen in the center area of the fracture surface. In essence, cracks expand along phase boundaries, leading to the formation of dimples. Combined with features in Figure 7b, more and finer dimples represent a more uniform plastic deformation in Ti-45551 samples under dynamic loading.

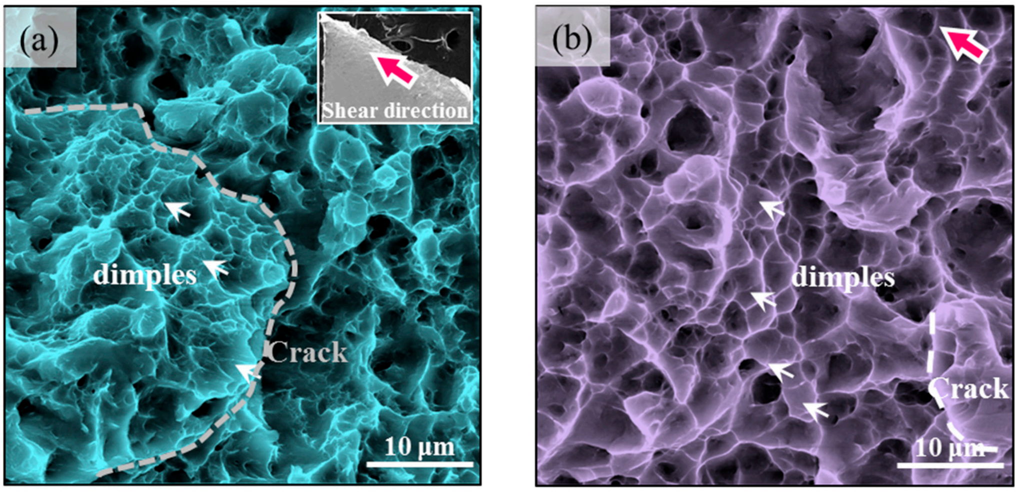

Figure 7. SEM images of fracture surface at (**a**) quasi-static loading condition, with inset showing the macro failure mode and (**b**) dynamic loading condition.

4. Conclusions

In the present work, we fabricated a lamellar α + β Ti-45551 alloy by two-stage aging, and systematically investigated the influence of the microstructure characteristics of lamellar α + β phases on tension deformation and failure at different strain rates. Both the strength and the ductility of the Ti-45551 alloy are higher under dynamic loading, because more dislocations are activated in both the α and β phase. The ductility of the Ti-45551 alloy is greatly controlled by the lamellar α phase. Fractographies of the lamellar α + β Ti-45551 alloy indicate a fracture mechanism mixture of dimples and cracks under tension loading. The increased and finer dimples shown in Ti-45551 samples at a high strain rate represent a more homogeneous plastic deformation. The lamellar α + β Ti-45551 alloy shows a positive strain-rate sensitivity with increasing strain rate. Both the strength and ductility of the Ti-45551 alloy are higher under dynamic loading, because more dislocations are activated in both the α and β phase. The ductility of the Ti-45551 alloy is greatly controlled by the lamellar α phase. Fractographies of the lamellar α + β Ti-45551 alloy indicate a fracture mixture mechanism of dimples and cracks under tension loading. The increased and finer dimples shown in Ti-45551 samples at a high strain rate represent a more homogeneous plastic deformation.

Author Contributions: Conceptualization, T.W. and X.L.; methodology, X.L. and Y.F.; validation, X.L. and Y.F.; formal analysis, T.W. and K.W.; investigation, T.W., S.S. and D.Y.; data curation, T.W.; writing—original draft preparation, T.W., S.S. and D.Y.; writing—review and editing, Y.F., K.W. and F.S.; project administration, F.S. All authors have read and agreed to the published version of the manuscript.

Funding: This research received no external funding.

Institutional Review Board Statement: Not applicable.

Informed Consent Statement: Not applicable.

Data Availability Statement: Not applicable.

Conflicts of Interest: The authors declare no conflict of interest.

References

1. Wang, Y.L.; Hao, M.Y.; Li, D.; Liang, Q.L.; Wang, D.; Zheng, Y.F.; Sun, Q.Y.; Wang, Y.Z. Enhanced mechanical properties of Ti-5Al-5Mo-5V-3Cr-1Zr by bimodal lamellar precipitate microstructures via two-step aging. *Mater. Sci. Eng. A* **2022**, *829*, 142117. [CrossRef]
2. Kolli, R.P.; Devaraj, A. A Review of Metastable Beta Titanium Alloys. *Metals* **2018**, *8*, 506. [CrossRef]
3. Qin, D.Y.; Zhao, F.; Li, Y.L. The conflicts between strength and ductility of bimodal Ti-5553 alloy with fine equiaxial prior β grains. *Mater. Sci. Eng. A* **2022**, *841*, 143074. [CrossRef]
4. Sauer, C.; Luetjering, G. Thermo-mechanical processing of high strength β-titanium alloys and effects on microstructure and properties. *J. Mater. Process. Technol.* **2001**, *117*, 311–327. [CrossRef]
5. Meyers, M.A.; Pak, H.R. Observation of an Adiabatic Shear Band in Titanium by High-Voltage Transmission Electron Microscopy. *Acta Metall.* **1986**, *34*, 2493–2499. [CrossRef]
6. Guo, S.; Meng, Q.K.; Zhao, X.Q.; Wei, Q.M.; Xu, H.B. Design and fabrication of a metastable β-type titanium alloy with ultralow elastic modulus and high strength. *Sci. Rep.* **2015**, *5*, 14688. [CrossRef]
7. Zherebtsov, S.V.; Murzinova, M.A.; Klimova, M.V.; Salishchev, G.A.; Popov, A.A.; Semiatin, S.L. Microstructure evolution during warm working of Ti-5Al-5Mo-5V-1Cr-1Fe at 600 and 800 °C. *Mater. Sci. Eng. A* **2013**, *563*, 168–176. [CrossRef]
8. Liu, S.F.; Li, M.Q.; Luo, J.; Yang, Z. Deformation behavior in the isothermal compression of Ti-5Al-5Mo-5V-1Cr-1Fe alloy. *Mater. Sci. Eng. A* **2014**, *589*, 15–22. [CrossRef]
9. Ma, W.; Wang, F.; Chen, B.H.; Li, B.; Zhang, X.Y.; Ma, M.Z.; Liu, R.P. Thermal compression behavior and microstructural evolution of Ti-30-5-3 alloys in lower α + β region. *Mater. Lett.* **2021**, *297*, 129876. [CrossRef]
10. Suri, S.; Viswanathan, G.B.; Neeraj, T.; Hou, D.H.; Mills, M.J. Room temperature deformation and mechanisms of slip transmission in oriented single-colony crystals of an α/β titanium alloy. *Acta Mater.* **1999**, *47*, 1019–1034. [CrossRef]
11. Zheng, Y.; Sosa, J.S.; Williams, R.E.A.; Wang, Y.; Banerjee, R.; Fraser, H.L. The role of omega phase in non-classical homogeneous precipitation of the alpha phase in beta-titanium alloys. *Scr. Mater.* **2016**, *111*, 81–84. [CrossRef]
12. Semiatin, S.L.; Bieler, T.R. The effect of alpha platelet thickness on plastic flow during hot working of Ti-6Al-4V with a transformed microstructure. *Acta Mater.* **2001**, *49*, 3565–3573. [CrossRef]
13. Lu, J.; Zhao, Y.; Ge, P.; Zhang, Y.; Niu, H.; Zhang, W.; Zhang, P. Precipitation behavior and tensile properties of new high strength beta titanium alloy Ti-1300. *J. Alloys Compd.* **2015**, *637*, 1–4. [CrossRef]
14. Santhosh, R.; Geetha, M.; Saxena, V.K.; Nageswararao, M. Studies on single and duplex aging of metastable beta titanium alloy Ti-15V-3Cr-3Al-3Sn. *J. Alloys Compd.* **2014**, *605*, 222–229. [CrossRef]
15. Huang, J.; Wang, Z.; Xue, K. Cyclic deformation response and micromechanisms of Ti alloy Ti-5Al-5V-5Mo-3Cr-0.5Fe. *Mater. Sci. Eng. A* **2011**, *528*, 8723–8732. [CrossRef]
16. Xu, Y.B.; Bai, Y.L.; Meyers, M.A. Deformation, Phase Transformation and Recrystallization in the Shear Bands Induced by High-Strain Rate Loading in Titanium and Its Alloys. *J. Mater. Sci. Technol.* **2006**, *22*, 737–746.
17. Ran, C.; Chen, P.W.; Li, L.; Zhang, W.F.; Liu, Y.L.; Zhang, X. High-strain-rate plastic deformation and fracture behaviour of Ti-5Al-5Mo-5V-1Cr-1Fe titanium alloy at room temperature. *Mech. Mater.* **2018**, *116*, 3–10. [CrossRef]
18. Clément, N.; Lenain, A.; Jacques, P.J. Mechanical property optimization via microstructural control of new metastable beta titanium alloys. *JOM* **2007**, *59*, 50–53. [CrossRef]
19. Mishra, A.; Martin, M.; Thadhani, N.N.; Kad, B.K.; Kenik, E.A.; Meyers, M.A. High-strain-rate response of ultra-fine-grained copper. *Acta Mater.* **2008**, *56*, 2770–2783. [CrossRef]
20. Meyers, M.A. *Dynamic Behavior of Materials*; Wiley-Interscience: New York, NY, USA, 1994; pp. 323–326.
21. Zheng, Z.; Waheed, S.; Balint, D.S.; Dune, F.P. Slip transfer across phase boundaries in dual phase titanium alloys and the effect on strain rate sensitivity. *Int. J. Plast.* **2018**, *104*, 23–38. [CrossRef]
22. Zheng, Z.B.; Balint, D.S.; Dunne, F.E. Investigation of slip transfer across HCP grain boundaries with application to cold dwell facet fatigue. *Acta Mater.* **2017**, *127*, 43–53. [CrossRef]
23. Li, X.Y.; Wei, Y.J.; Lu, L.; Lu, K.; Gao, H.J. Dislocation nucleation governed softening and maximum strength in nano-twinned metals. *Nature* **2010**, *464*, 877–880. [CrossRef] [PubMed]
24. Huang, C.W.; Zhao, Y.Q.; Xin, S.W.; Zhou, W.; Li, Q.; Zeng, W.D. Effect of microstructure on tensile properties of Ti-5Al-5Mo-5V-3Cr-1Zr alloy. *J. Alloys Compd.* **2017**, *693*, 582–591. [CrossRef]